Dynamics of plateau bursting in dependence on the location of its equilibrium

H. M. Osinga and K. T. Tsaneva-Atanasova
Bristol Centre for Applied Nonlinear Mathematics, Department of Engineering Mathematics, University of Bristol, Queen's Building, Bristol BS8 1TR, UK

Abstract: We present a mathematical analysis, based on numerical explorations, of the bursting patterns that arise in plateau-bursting models of endocrine cells as the position of the equilibrium varies. We consider both square-wave and pseudo-plateau bursting. Within the framework of systems with multiple time scales, it is well known how the underlying fast subsystem organises the behaviour of the model, but such results are valid only in a small enough neighbourhood of the singular limit that defines the fast subsystem. Hence, the slow variable (intracellular calcium concentration) must be very slow, while the physiologically realistic range is moderately slow. Furthermore, the theoretical predictions are also only valid for parameter values such that the equilibrium is close to a homoclinic bifurcation that occurs in the fast subsystem. In this paper, we discuss what happens outside this theoretically known neighbourhood of parameter space. Our results complement our earlier work, in collaboration with Rieß and Sherman (Journal of Theoretical Biology 2010, in press), which focussed on how the bursting patterns vary with the rate of change ε of the slow variable: we fix ε and move the equilibrium over the full range of the bursting regime.

Key words: plateau bursting, square wave, pseudo-plateau, subcritical and supercritical Hopf bifurcation, homoclinic bifurcation

In endocrine cells plateau bursting results in an increase in the intracellular calcium concentration ($[Ca^{2+}]_i$) and is essential for hormonal secretion [1, 2, 3]. The balance of inward (depolarising) and outward (repolarising) ionic currents governs repetitive rises (oscillations) in the intracellular calcium concentration (the slow variable) that are accompanied by plateau-bursting electrical activity in the membrane potential (the fast variable). There are two types of plateau bursting patterns that could be found in experimental as well as modelling studies. The classical square-wave [4, 5] (or fold-homoclinic [6]) bursting is typical for pancreatic β-cells and is characterised by well defined spikes in the active phase that are related to a family of stable periodic solutions in the fast subsystem. The other type of plateau bursting is typical for pituitary cells [7, 8, 9, 10, 11, 12] and has been classified in some studies as fold-subHopf [6] or pseudo-plateau bursting [11]. It is characterised by small irregular spikes in the active phase. There have been numerous modelling studies of plateau-bursting in a variety of endocrine cell types, including pancreatic β-cells [13, 14, 15] and pituitary cells [7, 8, 9, 10, 11, 12]. These models faithfully reproduce the distinct bursting patterns observed experimentally [7, 8, 10], but due to higher dimensions as well as inherent nonlinearities, it is rather difficult to analyze systematically the dynamics that underlies the plateau bursting regimes in these models.

Bursting activity manifests itself by periodic switches between an active (depolarised) phase and a silent (repolarised) phase. The main benefit of such prolonged electrical activity is its efficiency to increase intracellular Ca^{2+} in contrast to a single spike. Ultimately, this

results in an increase of $[Ca^{2+}]_i$ that participates in the stimulation of hormonal release from secretory vesicles [1, 2, 3]. Given the ubiquity of bursting firing it is of central importance to understand the way in which it is organised and how it emerges and dies. Moreover, different types of bursts are distinguished by their numbers of spikes, i.e., the duration of the active phase. The time of burst onset represents the temporal location of a certain stimulus feature, and the intra-burst spike count discriminates between different types of features. Therefore, it is crucial to dissect the mechanisms that govern the duration of the active phase, which is directly related to the number of spikes within a burst and, consequently, controls the timing and the amount of calcium entering the cell. We have recently shown in [16] that the dynamics of plateau bursters depends on the location of the full-system equilibrium point. The position of this equilibrium in bursting models is determined by the intersection between the slow-variable nullcline and the critical manifold of the full system. In general, parameter variations that affect the slow-variable nullcline or the critical manifold result in changes of the full-system equilibrium location. Among the most plausible physiologically relevant possibilities are variations in parameters describing the ionic currents that mediate bursting electrical activity such as ion channels conductances and gating properties. Another relevant physiological possibility is a perturbation in the slow-variable (calcium) dynamics that could be due to variations in calcium buffering capacity of the cells or calcium extrusion kinetics.

In order to investigate how plateau-bursting trajectories in the full system unfold as a function of a parameter that determines the location of its equilibrium we use here the polynomial plateau-bursting model introduced in [16] that can generate both types of plateau bursting. Our analysis of the bifurcations leading to plateau bursting in the full system of the polynomial plateau-bursting model extends and complements previous studies that have applied a standard fast-slow analysis [4, 5, 17, 18]. We find that both fold-subHopf and fold-homoclinic bursting can be readily interpreted as arising from bifurcations in the full system. In particular, we identify for both square-wave and pseudo-plateau bursters key roles for singular Hopf bifurcations that give rise to bursting via canard explosions as the position of the full-system equilibrium point changes. Furthermore, we study how the duration of the active phase is affected by the location of this equilibrium. In the case of square-wave bursting we clarify the mechanisms by which the bursting regime is born from canard trajectories in the full system as well as their role in spike adding. We also explain how the bursting regime disappears in tonic spiking as the equilibrium point traces the critical manifold. Finally, we show that the results obtained for pseudo-plateau bursting are extremely similar to those for square-wave bursting, despite the fact that the local theory close to the singular limit in a small neighbourhood of the homoclinic bifurcation predicts rather different behaviours. We end with a discussiong of the significance and potential implications of our results.

Results

Our analysis uses the polynomial plateau-bursting model introduced in [16]. It is a modified Hindmarsh-Rose model [19] that is given by the three-dimensional system of ordinary

differential equations

$$\left\{\begin{array}{rcrcl} \dot{x} &=& f(x,y,z) &:=& s\,a\,x^3 - s\,x^2 - y - b\,z, \\ \dot{y} &=& \phi\,g(x,y) &:=& \phi(x^2 - y), \\ \dot{z} &=& \varepsilon\,h(x,z) &:=& \varepsilon(s\,a_1\,x + b_1 - k\,z). \end{array}\right. \tag{1}$$

System (1) is a phenomenological model that, with the appropriate choice of parameters, can exhibit all common dynamical features found in a number of biophysical modelling studies of plateau bursting [20, 21, 7, 14, 22, 23, 15, 9, 10, 11]. In the context of plateau bursting, one should think of x as the membrane potential, y is the gating dynamics of the potassium (K^+) channels and z represents the dynamics of cytosolic Ca^{2+}. As in [16], we use $\phi = 1$ and consider ε a small positive parameter, so that z varies on a much slower time scale than x and y. This means that we can perform the classical analysis [4] where z is considered constant and treated as a parameter for the so-called fast subsystem in the (x, y)-plane. The parameters must be chosen such that the fast subsystem has a Z-shaped z-dependent family of equilibria and there exists a range of z-values for which there are two stable equilibria. Plateau bursting is then characterised by a Hopf bifurcation on the upper stable branch; the emanating family of periodic orbits is responsible for creating spikes in the active phase. For the case of square-wave bursting this Hopf bifurcation is supercritical and the stable limit cycles generate well-defined spikes. For pseudo-plateau bursting the Hopf bifurcation is subcritical, with unstable periodic orbits that lead to transient oscillations, which generate the small irregular spikes typical for this case. Without loss of generality, we obtain the above requirements by setting $a = 0.5$, $b = 1$, $a_1 = -0.1$ and $k = 0.2$; these are the same values as used in [16]. Hence, the only free parameters are s, b_1 and ε.

As mentioned before, the parameter ε controls the difference in time scales. The parameter s determines the criticality of the Hopf bifurcation; we consider $s = -1.61$ and $s = -2.6$ as representative choices for the square-wave and pseudo-plateau bursters, respectively, which are again the same choices as in [16]. The bifurcation diagrams for the fast subsystem with $s = -1.61$ and $s = -2.6$ are shown in Fig. 1(a) and (b), respectively. Both diagrams consist of a Z-shaped curve of equilibria in (x, y, z)-space, which form the critical manifold of (1); the equilibria are attracting where the curve is drawn as a solid line, saddles where the line is dashed, and repelling where it is dotted. For both cases there are four bifurcations along this Z-shaped curve: two fold (saddle-node) bifurcations labelled SN_1 and SN_2, a Hopf bifurcation labelled H, and a homoclinic bifurcation labelled HC that terminates the family of periodic orbits emanating from the Hopf bifurcation; this family of periodic orbits is drawn solid grey for the supercritical case (the periodic orbits are stable) and dotted grey for the subcritical case, where they are unstable.

The full system (1) has an equilibrium FP, which is a point on the curve in (z, x, y)-space that is defined by the family of equilibria for $\varepsilon = 0$. The location of FP is controlled by the parameter b_1 and FP persists as an equilibrium in this location for all ε. We can derive explicit expressions for when b_1 is such that FP is located at the bifurcation points SN_1, SN_2 and H; see the Appendix. The location at HC must be approximated numerically and the respective values of all four special locations for $s = -1.61$ and $s = -2.6$ are given to four decimal places in Table 1.

The study in [16] focused on the creation and bifurcations of bursting solutions (periodic orbits) for fixed s and b_1 with ε varying. Here, we consider s and ε fixed and investigate how

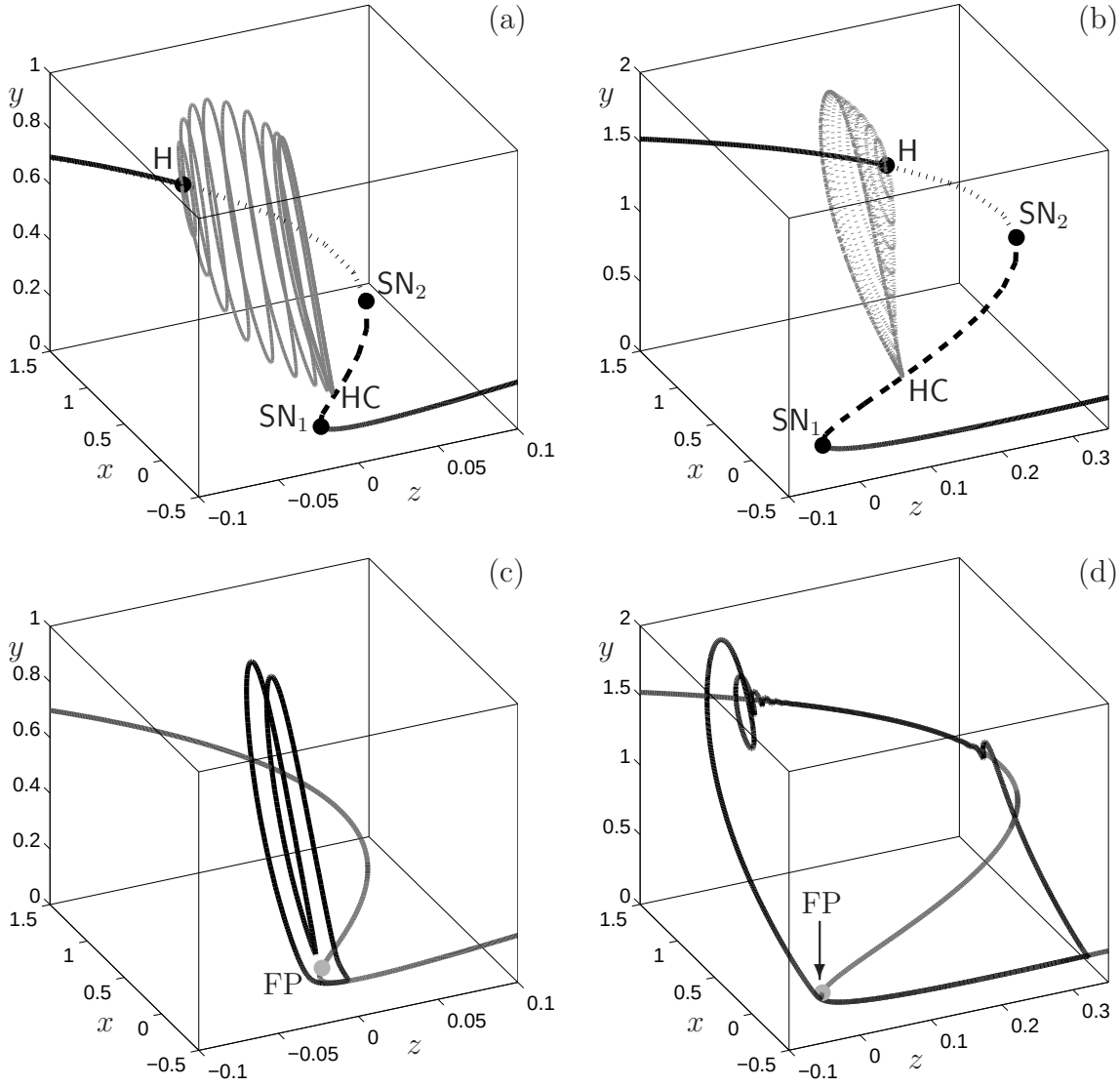

Figure 1: *Bifurcation diagrams of the fast subsystem of (1), where z is treated as a parameter, shown in (z, x, y)-space. The case for square-wave bursting, presented for $s = -1.61$ is shown in panel* (a) *and the case for pseudo-plateau bursting is presented for $s = -2.6$ in panel* (b)*. Solid, dashed, and dotted lines denote attracting, saddle, and repelling equilibria, respectively; the solid or dotted closed curves are selected from the family of periodic orbits emanating from a Hopf bifurcation* (H) *and terminating at a homoclinic bifurcation* (HC)*. The fold points are labelled* SN_1 *and* SN_2*. Panels* (c) *and* (d) *show examples of the plateau-bursting attractor and the (saddle) equilibrium FP of the full system for the representative value of $b_1 = -0.015$ with $s = -1.61$ and $s = -2.6$, respectively; the equilibrium branch from the corresponding panel* (a) *or* (b) *is included for reference.*

the bursting solution arises and subsequently changes as b_1 varies so that FP moves from the lower stable branch in (x, y, z)-space up along the middle (saddle) branch to the upper stable branch. We choose $\varepsilon = 0.01$ as a representative value for a realistic plateau-bursting model.

	$s=-1.61$				$s=-2.6$			
	b_1	x	y	z	b_1	x	y	z
SN_1	0	0	0	0	0	0	0	0
HC	-0.0279	0.1945	0.0378	0.0172	-0.0652	0.3672	0.1348	0.1514
SN_2	-0.0710	0.5052	0.2552	0.0519	-0.1415	0.8205	0.6732	0.3591
H	-0.1449	0.8409	0.7072	-0.0473	-0.2450	1.1003	1.2107	0.2053

Table 1: Values of b_1 and the corresponding locations of FP at the bifurcation points SN_1, HC, SN_2 and H for the two cases $s=-1.61$ and $s=-2.6$. The fold point SN_1 always lies at the origin with $b_1=0$; compare also Fig. 1. Explicit formulae for SN_1, SN_2 and H can be found in the Appendix.

We are particularly interested in how the dynamics changes as b_1 passes through the regime where FP is close to the fold points SN_1 and SN_2, the Hopf point H and, most importantly, the homoclinic bifurcation point, which acts as an organising center for the possible types of bursting solutions [24].

Bifurcations of the full-system equilibrium FP

The stability of FP changes as b_1 is varied. The real and imaginary parts of the three eigenvalues of FP as a function of b_1 are shown in Fig. 2 in rows (1) and (2), respectively; column 1 is for $s=-1.61$ and column 2 for $s=-2.6$. The changes in stability that occur as FP moves from the upper branch to the lower branch (which is for b_1 increasing, that is, from left to right in the figure) are the same for the supercritical case with $s=-1.61$ and the subcritical case with $s=-2.6$. For both values of s there is a bounded b_1-interval for which FP is a saddle and FP is stable otherwise. Due to the difference in time scales for system (1), we expect that one of the eigenvalues of FP is of order $O(\varepsilon)$. Figure 2 shows that this is indeed the case for both values of s and for almost all values of b_1; we indicate this eigenvalue by λ_ε.

Before we discuss the (plateau-)bursting solutions that exists particularly in the regime where FP is a saddle, we explain the two stability changes in some more detail. The changes in stability seem to happen when FP lies on H, which is at $b_1\approx-0.1449$ for $s=-1.61$ and $b_1\approx-0.2450$ for $s=-2.6$, and on SN_1 at $b_1=0$. Let us first consider the transition through the Hopf point H. For $b_1\ll 0$, the equilibrium FP has three stable eigenvalues, a pair $\lambda_1=\bar{\lambda}_2$ of complex conjugate eigenvalues with negative real parts and one real eigenvalue $\lambda_3<0$ that plays the role of λ_ε. As can be seen in Fig. 2, the pair $\lambda_1=\bar{\lambda}_2$ moves through the imaginary axis and becomes unstable. The transition happens at $b_1\approx-0.1457$ for $s=-1.61$ and $b_1\approx-0.2453$ for $s=-2.6$, that is, within an $O(10^{-3})$ distance from the b_1-value that corresponds to the Hopf bifurcation H of the fast subsystem. Hence, FP loses stability in a Hopf bifurcation H_{FP} at a distance $O(\varepsilon)$ from H, which similarly gives rise to a family of periodic orbits of the full system (1) that correspond to tonic spiking.

The equilibrium FP regains stability during the transition through the fold point SN_1. Figure 2 shows that the saddle FP with three real eigenvalues $\lambda_3<0<\lambda_2<\lambda_1$ before reaching SN_1 becomes a sink with three real eigenvalues $\lambda_3<\lambda_1<\lambda_2<0$ via a transition during which $\lambda_1=\bar{\lambda}_2$ are again complex conjugate. Hence, FP gains stability as the pair

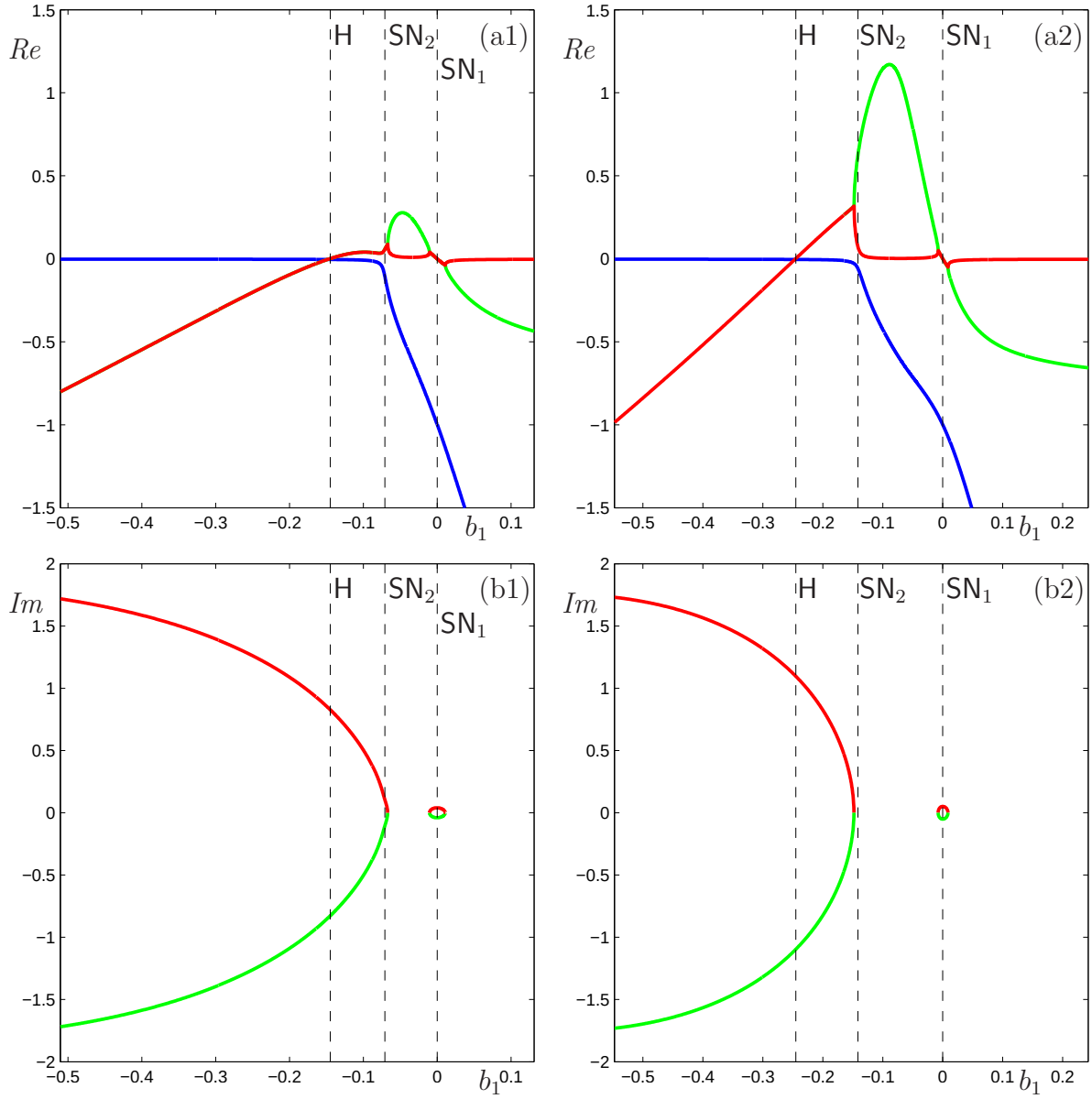

Figure 2: *Eigenvalues of the equilibrium FP of system (1) as* b_1 *varies; the case* $s = -1.61$ *is shown in panels* (a1) *and* (a2) *and* $s = -2.6$ *in panels* (b1) *and* (b2)*. Real and imaginary parts of the three eigenvalues are shown in rows 1 and 2, respectively. The vertical dashed lines indicate the* b_1*-values for which FP lies on the fold points* SN_1 *and* SN_2 *and the Hopf point* H*.*

$\lambda_1 = \bar{\lambda}_2$ pass through the imaginary axis, that is, again a Hopf bifurcation occurs. This transition is typical for systems with a fold point like SN_1 in the associated fast subsystem and it was described previously in [17, 18]. Note that λ_2 now plays the role of λ_ε and the transition is characterised by the fact that λ_1 becomes of the same order as λ_2. It seems that FP changes stability exactly at the fold point, but in fact, FP becomes stable already

at $b_1 = -0.26 \times 10^{-4}$ for $s = -1.61$ and $b_1 \approx -1.62 \times 10^{-4}$ for $s = -2.6$. We say that FP undergoes a *singular Hopf* bifurcation, denoted $\mathsf{SH}_{\mathrm{FP}}$, which is expected to occur $O(\varepsilon)$ away from the fold point of the fast subsystem [17, 25]. During this transition, when FP is $O(\varepsilon)$-close to SN_1, the slow-fast nature of the system changes from having one slow variable to having two slow variables. It is not hard to show that for our choice of parameters, $\mathsf{SH}_{\mathrm{FP}}$ always takes place at a value $b_1 < 0$; see the Appendix.

As mentioned above, as FP crosses H the role of λ_ε is played by λ_3, while during the crossing of SN_1 it is played by λ_1. The exchange of roles occurs as FP crosses SN_2. Essentially, what is happening is the following. The fold point SN_2 in the fast subsystem is characterised by the fact that one of the eigenvalues of the corresponding equilibrium of the fast system is zero. In the full system (1), however, there is no bifurcation. Instead, two eigenvalues of the full system come very close to zero and their corresponding (real parts) of the eigenvectors almost align. Similarly to the singular Hopf bifurcation, this means that the slow-fast nature of the system changes from having one slow variable to having two slow variables. For the case $s = -2.6$ we can see this clearly in Fig. 2(b1), because all three eigenvalues are real before b_1 increases past the value at SN_2 and the two near zero come very close together. The process for $s = -1.61$ shown in Fig. 2(a1)-(a2) is more complicated: the two unstable eigenvalues are complex conjugate and the real parts of all three eigenvalues remain close to zero as FP crosses SN_2, after which there is a clear divergence from zero for all three eigenvalues. Perhaps for this case the system loses its slow-fast nature altogether during the transition through SN_2.

The two Hopf bifurcations of FP as b_1 varies and s and ε are fixed, give rise to a regime of (plateau-)bursting solutions. The analysis in [16] showed that the ε-dependence of the bursting solutions is not affected by the criticality of H, that is, system (1) exhibits the same sequence of bifurcations to different types of bursting solutions for $s = -1.61$ as well as $s = -2.6$. However, the location of FP relative to the homoclinic bifurcation HC matters. Indeed, Terman [26] and Belykh *et al.* [24] studied how HC organises the bursting solutions for small ε and discussed the transitions from tonic spiking to square-wave bursting in a small neighbourhood around HC. However, pseudo-plateau bursting has not been treated in the same detail. In [16] we reported that the case of pseudo-plateau bursting is reminiscent of *Scenario 1* described in [24], which corresponds to relaxation oscillations. This means that there is no tonic spiking in a neighbourhood of HC, provided ε is small enough. Instead, pseudo-plateau bursting solutions are observed throughout the transition through HC, but the oscillations in the active phase have exponentially small amplitudes. Here, we fix $\varepsilon = 0.01$ to a moderately small value and show how the bursting solutions are organised as b_1 varies over a large range so that FP moves well outside a neighbourhood of HC. We first treat the cases $s = -1.61$ and $s = -2.6$ separately and end with a discussion of our findings. In particular, the choice for s, that is, the criticality of the Hopf bifurcation H, again does not influence the bifurcation diagram. Therefore, this paper complements the discussion in [16], where ε was the main bifurcation parameter and b_1 remained fixed.

Transitions to bursting solutions for $s = -1.61$

Let us begin with the case of square-wave bursting, where $s = -1.61$. This case is characterised by the fact that the Hopf bifurcation H of the fast subsystem is supercritical; see

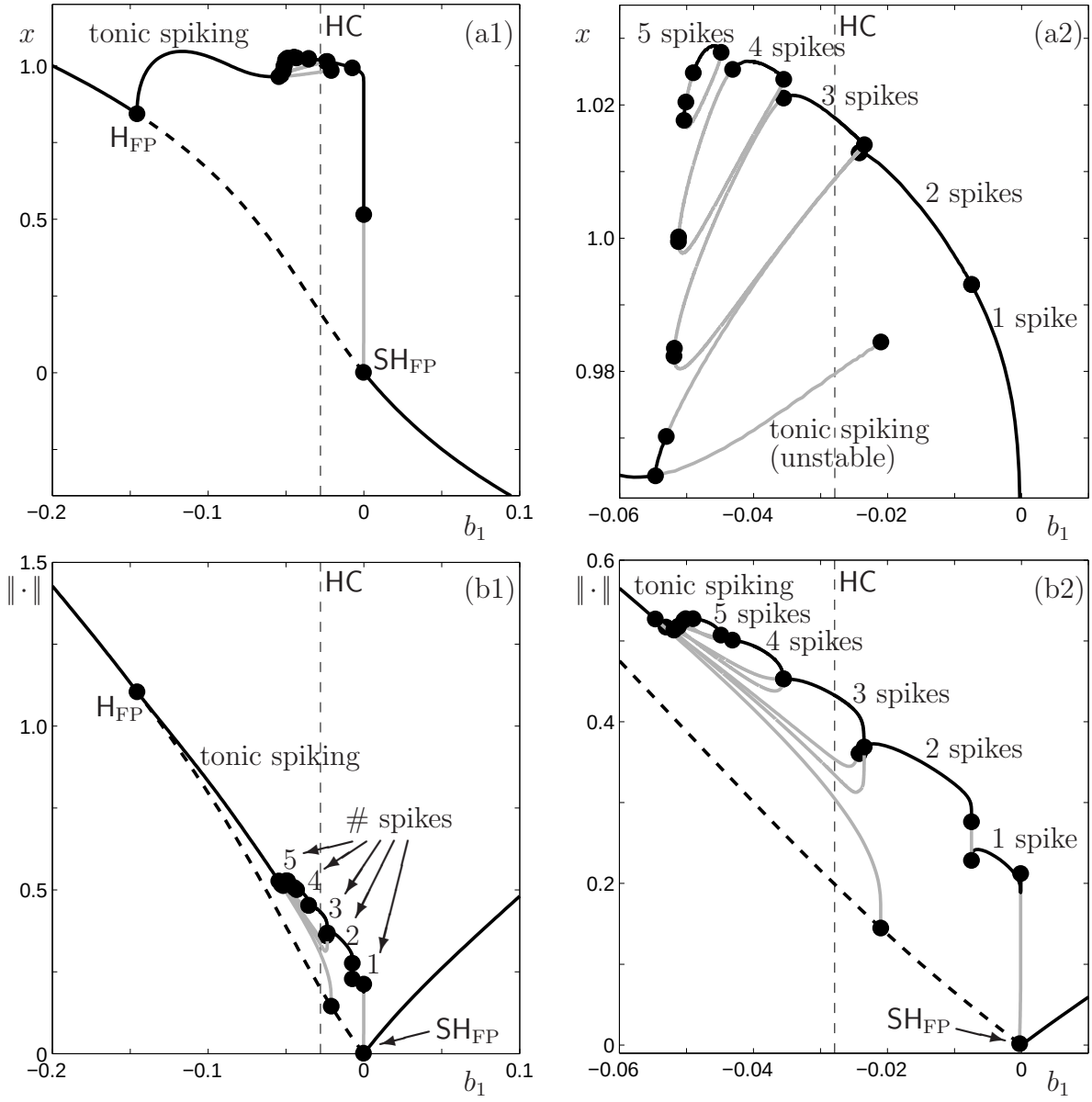

Figure 3: *Bifurcation diagram of system (1) with* $s = -1.61$, $\varepsilon = 0.01$ *and* b_1 *varying. Row 1 shows* x *versus* b_1*, with periodic orbits indicated by their maximal* x*-values; row 2 shows the AUTO* L_2*-norm versus* b_1*. Column* (b) *shows enlargements of the bursting region. The one- and two-spike solutions are connected to the family of tonic spiking via period-doubling bifurcations; we also found three isolas with the three-, four- and five-spike solutions.*

Fig. 1(a). According to [24, 26, 16], the expected type of bursting solution depends on the location of FP relative to the homoclinic bifurcation HC of the fast subsystem, which occurs at $b_1 = b_{\rm HC} \approx -0.0279$. For $b_1 > b_{\rm HC}$ we expect to see square-wave bursting as soon as ε is small enough, and for $b_1 < b_{\rm HC}$ we expect to see tonic spiking, again provided ε is small enough. In fact, Terman [26] gives a very detailed description of the transitions that occur

in a small interval $[b_{\rm HC}-\delta, b_{\rm HC}+\delta]$, with $0<\delta\ll 1$, for small enough fixed ε; see Fig. 9 in [26], where k acts as $-b_1$ in our context. Since our choice $\varepsilon=0.01$ is not very small, we expect a transition regime that is much simpler, but consistent with Fig. 9 in [26].

Figure 3(a1) and (b1) show two different projections of the bifurcation diagram of system (1) for $s=-1.61$ with associated enlargements of the bursting region in column (2). Row (a) shows the projection in the (b_1,x)-plane, where periodic orbits are represented by their maximum x-value. Row (b) shows the L_2-norm $\|\cdot\|$ that is standard in AUTO [27]; it is the standard Euclidean norm $\|(x,y,z)\|_{\rm E}=\sqrt{x^2+y^2+z^2}$ for points $(x,y,z)\in\mathbb{R}^3$ and defined as

$$\|\mathbf{u}\|=\frac{1}{T}\int_0^1 \|\mathbf{u}(s\,T)\|_{\rm E}\ ds,$$

for a periodic orbit $\mathbf{u}=\{\mathbf{u}(t)\in\mathbb{R}^3 \mid 0\le t\le T\}$ with period $T>0$. As before, the curve that corresponds to the equilibrium FP is dashed in between the two Hopf bifurcations $\mathsf{H}_{\rm FP}$ and $\mathsf{SH}_{\rm FP}$, where FP is a saddle. The thin vertical black dashed line lies at $b_1=b_{\rm HC}$. The Hopf bifurcations give rise to two families of periodic orbits that are, in fact, connected. This connected family contains the tonic spiking solutions as well as plateau (square-wave) bursting with one and two spikes. The enlargements in Figs. 3(a2) and (b2) show that there are three further disjoint families of three- four- and five-spike solutions, respectively. The transitions between these different bursting solutions are detailed below.

The tonic (continuous) spiking solutions for $b_1<b_{\rm HC}$ arise from the Hopf bifurcation $\mathsf{H}_{\rm FP}$ of FP, which for $s=-1.61$ occurs at $b_1\approx -0.1457$. A selection of the periodic orbits along this branch is shown in Fig. 4. Panel (a) shows the time series for x; here the periods T of the orbits are rescaled to 1 such that each orbit covers the $[0,1]$ interval. A three-dimensional view of the family in (z,x,y)-space is shown in Fig. 4(b). The Hopf bifurcation $\mathsf{H}_{\rm FP}$ is supercritical and, initially, the periodic orbits are small-amplitude sinusoidal oscillations; in fact, they are almost planar with z almost constant. In physiological models such planar oscillations of the membrane potential are related to negligible variations of the intracellular calcium concentration, which has virtually no effect on secretion [2, 28]. As b_1 increases, the amplitude of the oscillations grows to a size that is similar to that of the homoclinic orbit of the fast subsystem at HC, but the periodic orbits are still close to planar. In the singular limit, as $\varepsilon\to 0$, each periodic orbit in this family converges to one of the periodic orbits in the family that exists in the fast subsystem with z constant; for example, see [18]. For our value of $\varepsilon=0.01$, a supercritical period-doubling bifurcation (PD) occurs at $b_1\approx -0.0547$, after which the family is unstable; the periodic orbit corresponding to this bifurcation is labelled PD_1 and drawn with a thicker curve in Fig. 4. The unstable family ends in a homoclinic bifurcation at $b_1\approx -0.0210$, which is $O(\varepsilon)$-close to $b_{\rm HC}\approx -0.0279$; the equilibrium FP for b_1 at this homoclinic bifurcation is also shown in Fig. 4(b). The unstable periodic orbits have b_1-values very close to $b_{\rm HC}$ and their profiles exhibit well-defined (single) spikes, rather than sinusoidal oscillations; see Fig. 4(a).

The family of period-doubled attracting periodic orbits that emanates from PD_1 consist of two-spike solutions. These do not correspond to two-spike plateau bursting, because there is no clear silent phase in these oscillations and there are no significant variations of the slow variable. The period-doubled family becomes unstable in a second supercritical PD, labelled PD_{21}, that occurs at $b_1\approx -0.0531$, and regains stability in another PD at $b_1\approx -0.0242$

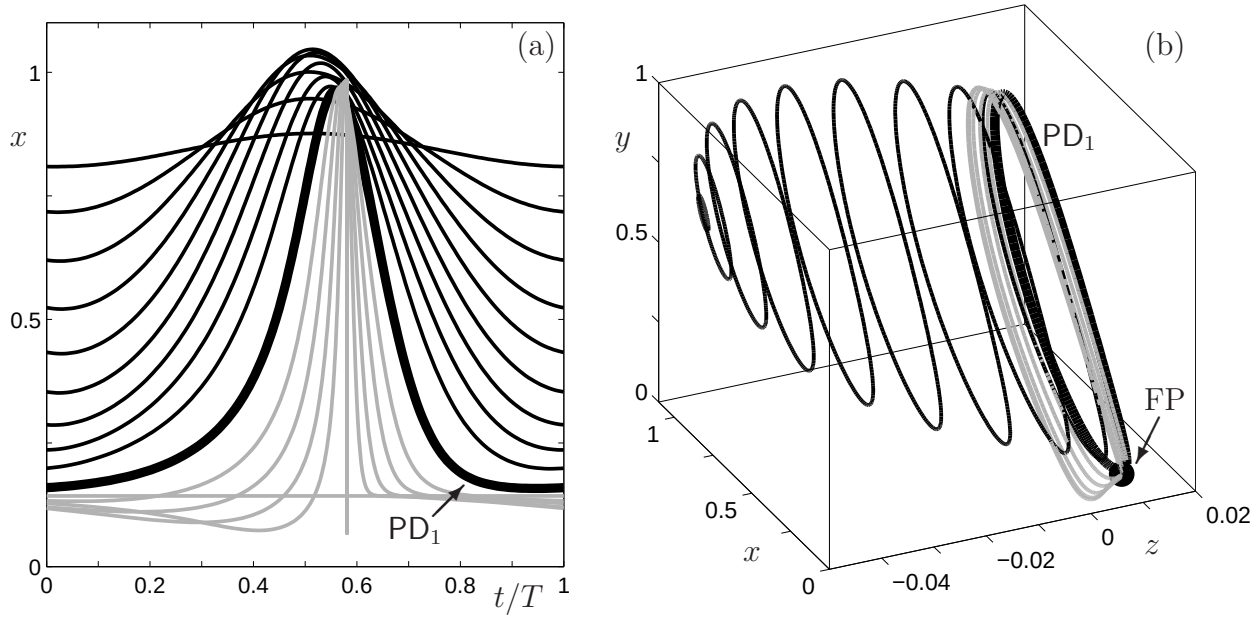

Figure 4: *Selected periodic orbits of system (1) with* $(s, \varepsilon) = (-1.61, 0.01)$ *and* $b_1 \in [-0.1454, -0.0210]$ *from the regime of tonic spiking in Fig. 3. Stable orbits are black, unstable ones grey, and the orbit at the period-doubling bifurcation for* $b_1 \approx -0.0547$ *is shown using a thicker curve. Panel* (a) *shows time series of the* x*-coordinate, where the periods are scaled to 1. Panel* (b) *shows the corresponding orbits in* (z, x, y)*-space with FP plotted for* $b_1 = -0.0210$ *approximately at which the primary family ends in a homoclinic bifurcation.*

(PD_{22}), which is now subcritical. Note that this second stable segment of the family of period-doubled periodic orbits lies on the other side of b_{HC}, that is, FP has crossed HC. The orbits along this second stable segment are two-spike bursting solutions. Figure 5 illustrates the transition from doubled tonic spiking to two-spike bursting via the segment of unstable periodic orbits (coloured grey). Such two-spike bursting solutions are accompanied by larger variations in the slow variable that in physiological models could be more significant in terms of hormonal secretion. As before, the (scaled) time series for x are shown in panel (a) and the corresponding phase portraits in panel (b). The orbits at the moment of the PDs are drawn with thicker curves. Figure 5(b) shows the gradual development of a silent-phase segment for the family of unstable periodic orbits.

The two supercritical PDs labelled PD_1 and PD_{21} appear to be the start of a period-doubling cascade to a chaotic attractor. As predicted in [26], we expect to see chaotic spiking solutions before FP passes through HC, and indeed, none of the attractors in the period-doubling cascade persist until $b_1 = b_{\mathrm{HC}}$. As mentioned above, the primary family that emanates from H_{FP} ends at a homoclinic bifurcation, but the branches emanating from the subsequent PDs seem to pass through this b_1-value and regain stability in subcritical PDs that are quickly followed by folds of periodic orbits (SNP). For example, the family emanating from PD_{22} undergoes an SNP at $b_1 \approx -0.0235$ that is almost immediately followed by a PD, before connecting to the corresponding branch from the period-doubling cascade. Hence,

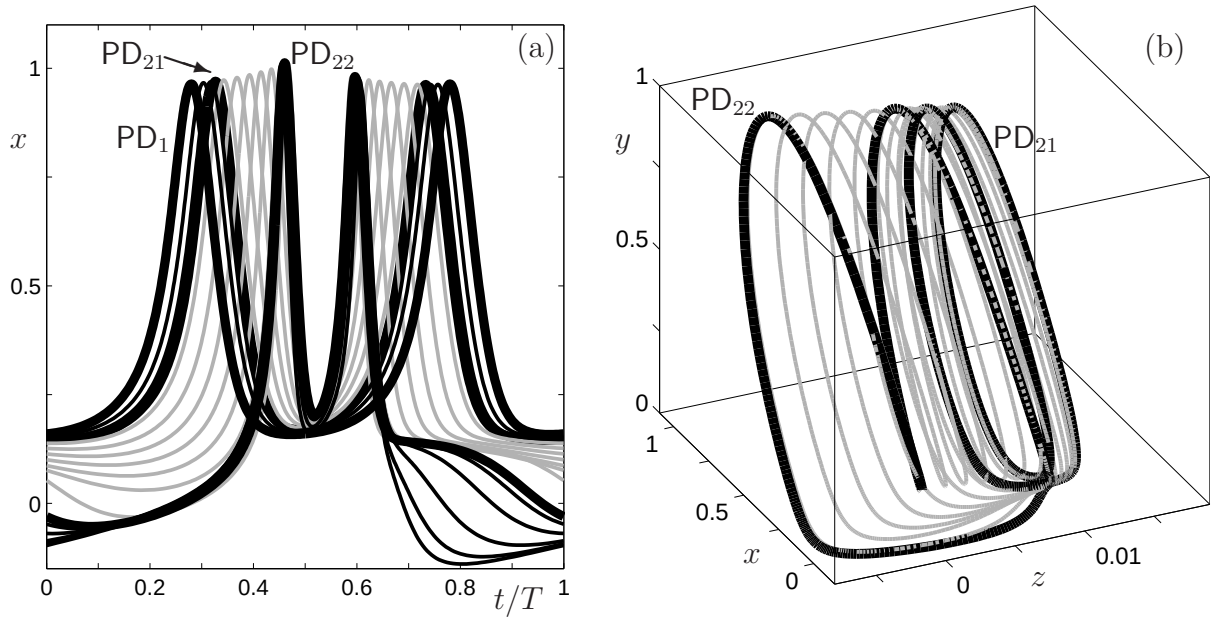

Figure 5: *Selected stable (black) and unstable (grey) periodic orbits of system (1) with* $(s, \varepsilon) = (-1.61, 0.01)$ *along the period-doubled branch emanating from* PD_1 ($b_1 \approx -0.0547$) *in Fig. 4, illustrating the transition from doubled tonic spiking to two-spike bursting solutions. Panel* (a) *shows time series of the* x*-coordinate with the periods scaled to 1. Panel* (b) *shows the periodic orbits corresponding to the unstable segment in between the two period-doubling bifurcations* PD_{21} ($b_1 \approx -0.0531$) *and* PD_{22} ($b_1 \approx -0.0242$) *in* (z, x, y)*-space.*

there appears to exist a period-doubling cascade "back" comprising subcritical PDs and SNPs.

The two-spike bursting solutions are part of the family that emanates from the singular Hopf bifurcation $\mathsf{SH}_{\mathrm{FP}}$ that we detected at $b_1 \approx -2.63 \times 10^{-4}$. This singular Hopf bifurcation is subcritical, so at first, this family is unstable. The periodic orbits in this family are initially nearly circular and almost planar small-amplitude oscillations. The periodic orbits become stable after an SNP at $b_1 \approx -1.31 \times 10^{-4}$. The amplitudes of the periodic orbits increases very rapidly and the family grows into a large-amplitude single-spike bursting attractor within an $\mathrm{O}(10^{-7})$ parameter interval; this rapid transition is called a canard explosion and is typical after a singular Hopf bifurcation [25]. Figure 6(a) is an enlargement of the canard explosion from the bifurcation diagram in Fig. 3(a). Panel (b) shows a selection of the periodic orbits from this canard explosion, where the unstable periodic orbits are coloured grey and the thicker black curve is the periodic orbit at the moment of the SNP. Note that the attracting (black) periodic orbits are no longer planar.

The canard explosion is organised by attracting and saddle slow manifolds associated with the critical manifold formed by the attracting and saddle branches of the Z-shaped curve of equilibria of the fast subsystem of (1). Each branch of the critical manifold, away from the fold points SN_1 and SN_2, gives rise to a slow manifold with the same stability type. These slow manifolds are orbit segments that remain $O(\varepsilon)$-close to the critical manifold

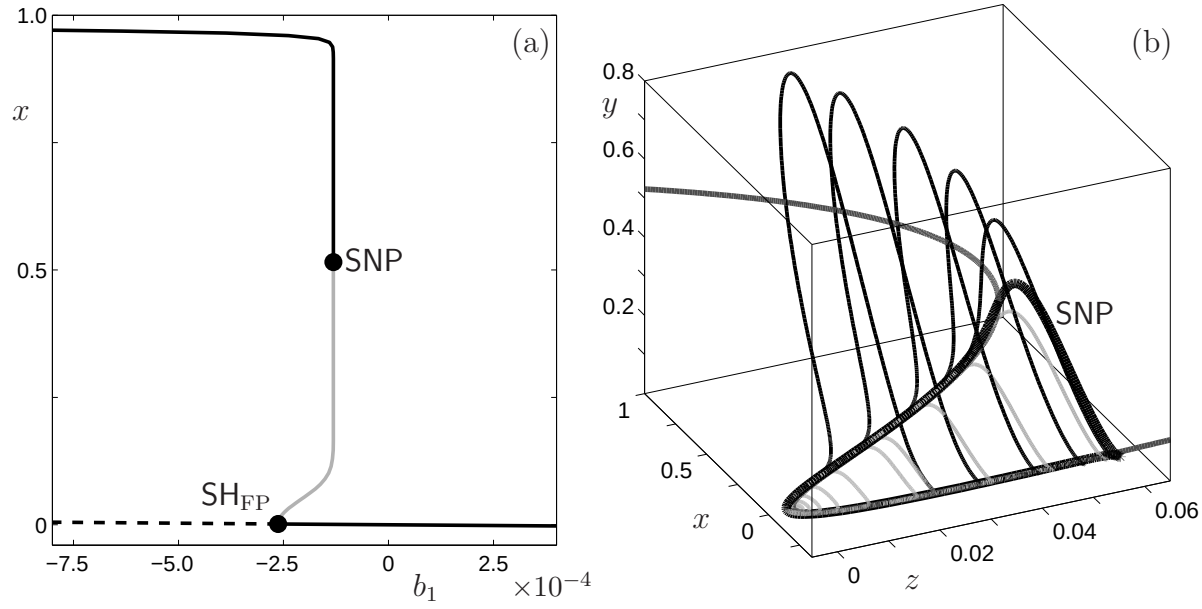

Figure 6: *Enlargement of the bifurcation diagram in the* (b_1, x)*-plane near the canard explosion from the singular Hopf bifurcation* $\mathsf{SH}_{\mathrm{FP}}$*. Selected stable (black) and unstable (grey) periodic orbits are shown in panel (b) together with the Z-shaped equilibrium branch from the fast subsystem of (1).*

for $O(1)$ time. Consider the attracting and saddle slow manifolds associated with the two branches that meet at SN_1. As an approximation, we plotted the Z-shaped equilibrium curve in Fig. 6(b) to illustrate how the periodic orbits are formed by segments that closely follow the attracting slow manifold as well as the saddle slow manifold, and close with a near-linear segment along a fast direction. Initially, the periodic orbits always close via a short fast segment back to the attracting slow manifold. Their amplitude increases such that the periodic orbits contain increasingly longer segments that follow the saddle slow manifold. However, the family of periodic orbits does not end when the point near SN_2 at the other end of the saddle slow manifold is reached. Instead, the periodic orbits stabilise and develop a large-amplitude spike that results from the fact that the jump happens in the opposite fast direction. The SNP separates the "jump-back" from "jump-away" periodic orbits. The periodic orbit that corresponds to the SNP point is called a *maximal canard* that is formed by the intersection (coincidence) of the attracting and saddle slow manifolds when extended past SN_1; see [25] for more details.

The single-spike bursting attractor acquires an additional spike in a rather similar process involving two SNPs at almost the same b_1-value $O(10^{-7})$ close to $b_1 = -7.458 \times 10^{-3}$. This process was described in [21] and revisited in [29], where the slow manifolds have been computed for a FitzHugh–Nagumo model and the transitions are nicely illustrated. The resulting two-spike bursting attractor connects to the branch of stable periodic orbits from the period-doubling bifurcation at $b_1 \approx -0.0242$. Terman [21] called such a succession of two SNPs a *spike-adding* bifurcation and studied them in the context of decreasing ε. In theory, as ε decreases a series of spike-adding bifurcations turns the two-spike plateau burster into an

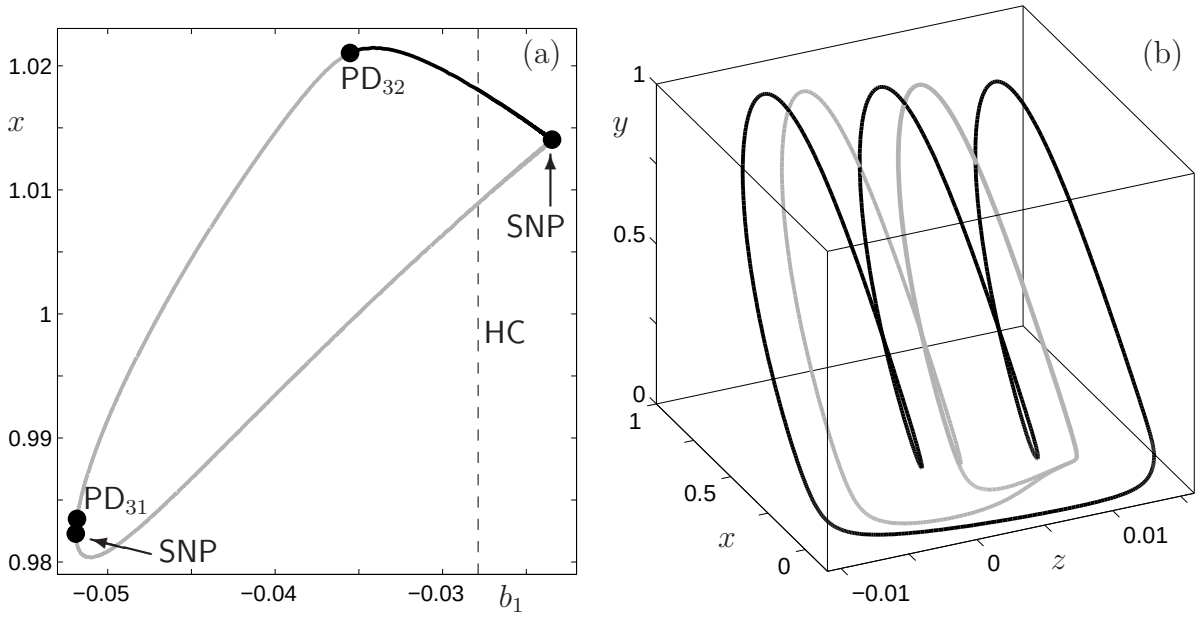

Figure 7: *Isola of three-spike periodic orbits* (a) *for system (1) with* $(s, \varepsilon) = (-1.61, 0.01)$. *Panel* (b) *shows the stable (black) and unstable (grey) periodic orbits* (b) *for* $b_1 = b_{\rm HC} \approx -0.0279$, *that is, such that FP lies at* HC.

n-spike plateau burster, where $n \to \infty$ as $\varepsilon \to 0$. However, for our fixed choice of $\varepsilon = 0.01$, we only have this one spike-adding bifurcation. Instead, as FP changes its position, additional spikes are created via isolas and we were able to find three. Figure 7 shows the isola for three-spike solutions, which is representative for the four- and five-spike isolas. Panel (a) shows the bifurcation diagram in the (b_1, x)-plane. The range in b_1 of the isola is marked by two SNP bifurcations. The bottom branch consists of saddle three-spike solutions and the top branch on either end is initially stable. In particular, most of the top segment of the isola is stable. The three-spike bursting solutions at both ends of the branch lose stability in PDs at PD_{31} and PD_{32}. Figure 7(b) shows the stable and unstable pair of periodic orbits on the isola for $b_1 = b_{\rm HC}$. Both periodic orbits have three spikes; the second and third spike of the unstable (grey) orbit are almost the same. Indeed, this solution lies very close to one of the unstable period-doubled solutions discussed in Fig. 5. Note that these period-doubled solutions are non-orientable, while the saddle three-spike solutions on this lower branch are orientable.

Transitions to bursting solutions for $s = -2.6$

Let us now consider the case of pseudo-plateau bursting, where $s = -2.6$. In contrast to the case for $s = -1.61$, the Hopf bifurcation H of the fast subsystem of (1) is now subcritical; see Fig. 1(b). As discussed in [16], this case is very much like *Scenario 1* in [24], where the Z-shaped equilibrium curve of the fast subsystem does not contain a Hopf bifurcation point H. For $0 < \varepsilon \ll 1$, *Scenario 1* gives rise to large-amplitude relaxation oscillations, irrespective of location of FP relative to HC. For our case, the presence of H leads to an additional *delayed*

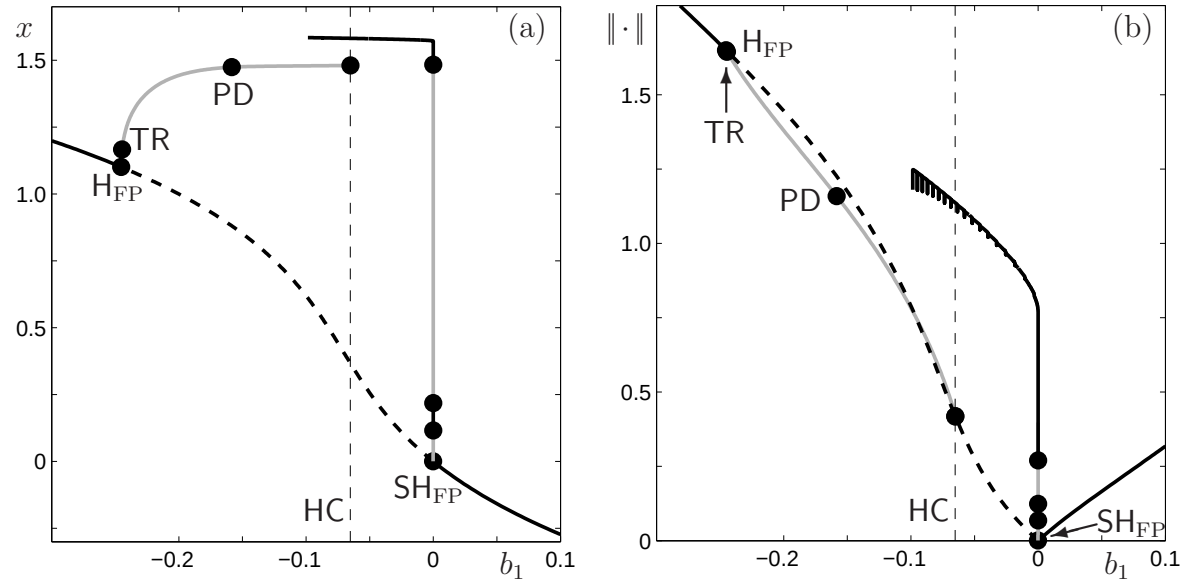

Figure 8: *Bifurcation diagram of system (1) with* $s = -2.6$, $\varepsilon = 0.01$ *and* b_1 *varying. Panel (a) shows* x *versus* b_1*, with periodic orbits indicated by their maximal* x*-values; panel (b) shows the AUTO* L_2*-norm versus* b_1*. The bursting region persists for lower values of* b_1 *and was halted due to numerical difficulties. This branch of pseudo-plateau bursting orbits loses its silent phase as* b_1 *decreases further, and eventually connects to the family that emanates from the Hopf bifurcation* H_{FP} *at* $b_1 \approx -0.2453$*.*

passage through a Hopf bifurcation in the active phase: the oscillation exhibits high-frequency bursts with amplitudes that are exponentially small, except for the first and last spikes at the beginning and end of the active phase. If ε is only moderately small, the bursting frequency decreases and the decay in their amplitudes is no longer exponential; this case is described as the passage through a *tourbillion* in the discussion on the *dynamic Hopf* bifurcation in [25]. Our choice for $\varepsilon = 0.01$ in (1) still leads to pseudo-plateau bursting of relaxation-oscillation type; pseudo-plateau bursting as a tourbillion can be found, for example, in [12, 11].

Figure 8 shows the bifurcation diagram of system (1) for $s = -2.6$ and should be compared with Fig. 3. As before, the vertical axis in row (a) is x and in row (b) it is the AUTO L_2-norm $\|\cdot\|$; the second column shows enlargements of the bursting region. The equilibrium branch FP is the black curve with a dashed segment in between the two Hopf bifurcations H_{FP} and $\mathsf{SH}_{\mathrm{FP}}$, where FP is a saddle; we detected these at $b_1 \approx -0.2453$ and $b_1 \approx 1.620 \times 10^{-4}$, respectively. As for the case with $s = -1.61$, we find that H_{FP} is supercritical and $\mathsf{SH}_{\mathrm{FP}}$ is subcritical. We believe that the emanating families of periodic orbits are again connected, but unfortunately, our numerical continuation methods are unable to resolve this connection; we discuss the missing transitions with the help of numerical simulations.

Just as for $s = -1.61$, the family of periodic orbits that emanates from H_{FP} corresponds to tonic spiking. However, it loses stability at $b_1 \approx -0.2446$ in a torus bifurcation (TR) rather than a PD. In fact, the unstable family past the torus bifurcation undergoes a PD at $b_1 \approx -0.1583$ before ending in a homoclinic bifurcation at $b_1 \approx -0.0651$; note that this

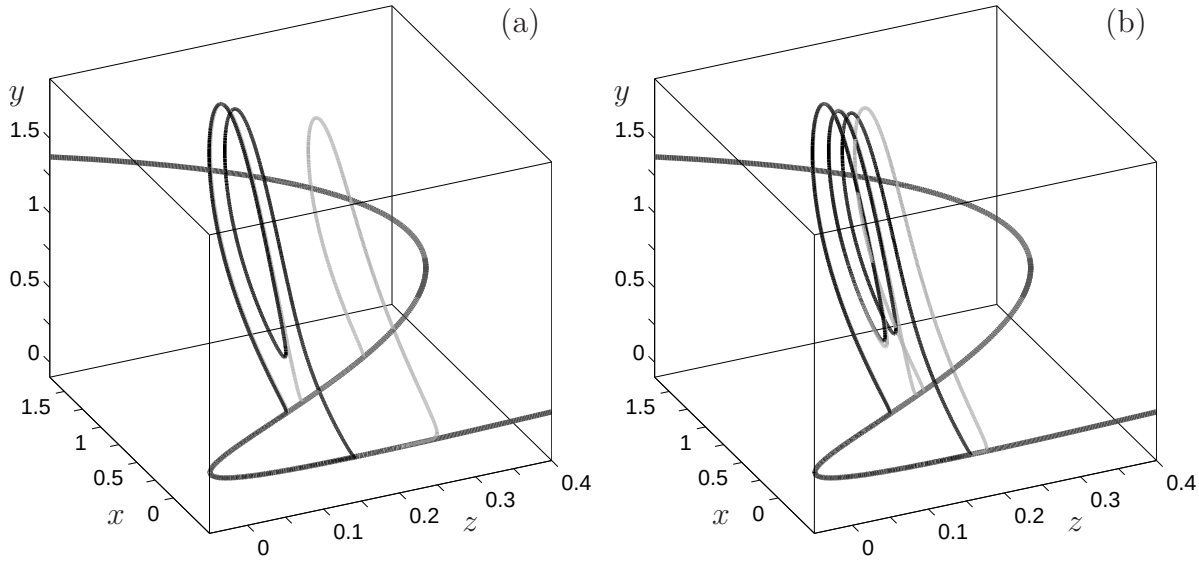

Figure 9: *Transitions from n-spike periodic orbits to pseudo-plateau bursting with n oscillations in system (1) with* $(s, \varepsilon) = (-2.6, 0.01)$ *and* $b_1 \approx -0.299 \times 10^{-4}$. *Shown are the transitions for* $n = 2$ (a) *and* $n = 3$ (b).

homoclinic bifurcation is again $O(\varepsilon)$-close to $b_{\rm HC}$. It seems that the torus bifurcation is subcritical, but nearby attracting solutions exist, even for $b_1 < -0.2446$ that are seemingly nonperiodic. In terms of tonic-spiking behaviour, these attractors are very similar to the coexisting attracting periodic orbit; the only essential difference is the (in)commensurability between the periods of the x- (or y-) and z-oscillations.

The singular Hopf bifurcation $\mathsf{SH}_{\rm FP}$ at $b_1 \approx 1.620 \times 10^{-4}$ again gives rise to a canard explosion in an $O(10^{-7})$ interval near $b_1 \approx -0.299 \times 10^{-4}$. As before, the family is unstable at first, because $\mathsf{SH}_{\rm FP}$ is again subcritical; an SNP at $b_1 \approx -0.2992 \times 10^{-4}$ renders the family stable after which the periodic orbits are one-spike solutions. In contrast to the situation for $s = -1.61$, many spike-adding bifurcations occur within this same $O(10^{-7})$ parameter interval. Each time a spike is added, the periodic orbit transforms from a pseudo-plateau bursting orbit with n oscillations into one with $n+1$ oscillations; this transition is shown for $n = 2$ and 3 in Fig. 9; note that we had real difficulties resolving the stability of these orbits numerically, and the different colours are used merely to distinguish between the pairs of periodic orbits in each panel. The family remains virtually vertical until the periodic orbits contain many oscillations, almost all of them with extremely small amplitudes.

The many spike-adding bifurcations and the large number of small-amplitude bursting oscillations make it a challenge to continue the family in AUTO. In particular, the duration of the active phase lengthens relative to the duration of the silent phase as b_1 decreases. The continuation breaks down at $b_1 \approx -0.1025$ and we had to resort to simulations for smaller b_1-values. The relative duration of the silent phase shrinks to zero and for $b_1 \approx -0.2445$ the periodic orbit becomes a tonic spiking solutions without a silent phase. Figure 10 shows time series of x for $b_1 = -0.21$, $b_1 = -0.24$ and $b_1 = -0.2446$ in panels (a), (b) and (c), respectively; the orbit in Fig. 10(c) intersects the plane $\{y = 1.2\}$ in two seemingly disjoint

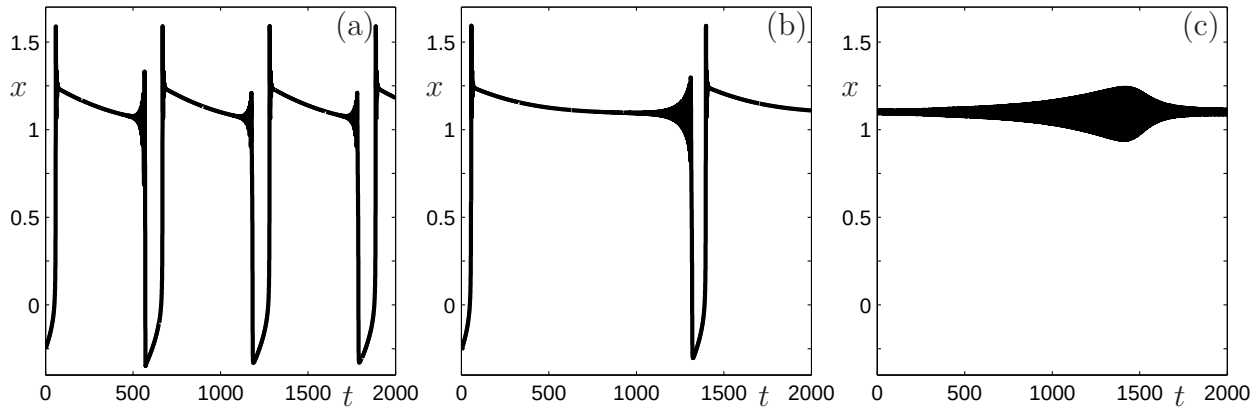

Figure 10: *Time series for the x-coordinate of attractors in system (1) with $(s, \varepsilon) = (-2.6, 0.01)$ for $b_1 = -0.21$, -0.24, and -0.2446 in panels* (a), (b), *and* (c), *respectively; the orbit in panel* (c) *appears to lie on a torus.*

closed curves, which indicates that it lies on a quasi-periodic invariant torus. Since these orbits were obtained via simulations, it is not clear whether they are part of the branch shown in Fig. 8.

In order to investigate whether the pseudo-plateau bursting solutions are indeed connected to the family of tonic spiking solutions, we calculated the bifurcation diagram for $\varepsilon = 0.01$. For this larger value of ε, the family emanating from the singular Hopf bifurcation ends in a homoclinic bifurcation and additional isolas exist with larger numbers of bursting oscillations; this is very similar to the bifurcation diagram for $s = -1.61$ shown in Fig. 3. We remark that for $s = -1.61$ in Fig. 3, the branch emanating from PD_1, which connects the tonic spiking solutions with the square-wave bursting solutions via the two PDs PD_{21} and PD_{22}, splits into two separate families that both end in homoclinic bifurcations when we choose $s = -1.6$ instead of $s = -1.61$ (not shown). Before the branch for $s = -2.6$ with $\varepsilon = 0.01$ ends in a homoclinic bifurcation, there is also a PD. Hence, we believe that there is a family of periodic orbits that connects the pseudo-plateau bursting solutions with tonic spiking via PDs that sit much higher in the period-doubling cascade and involves periodic orbits that are all unstable. The coexisting attracting periodic orbits are likely organised in isolas, much like the bifurcation diagram for $s = -1.61$.

Discussion

Due to the importance of bursting electrical activity in neuroendocrine cells there has been an immense interest in analysing plateau-bursting models. Previous studies of the effects of changing the location of the full-system equilibrium have been performed only for square-wave bursters and applied a standard fast-slow analysis [30, 20, 26, 31]. These studies primarily focussed on the effects of changing the rate of decay of calcium (through varying calcium pump rates) inspired by the ability of this parameter to convert bursting to small-amplitude tonic spiking in the first biophysical model of square-wave bursting [13]. Experi-

mentally, however, conversion from bursting to spiking and vice versa has been observed by blocking Ca^{2+}-sensitive potassium channels. In particular, a blockade of small-conductance Ca^{2+}-sensitive K^+-channels (SK) in pituitary gonadotrophs [32] or in pancreatic β-cells [33] results in transitions to small-amplitude continuous spiking riding on a depolarised plateau. In contrast, a blockade of large-conductance Ca^{2+}-sensitive K^+-channels (BK) in pituitary somatotrophs has been shown [8] to convert pseudo-plateau bursting to large-amplitude continuous spiking that could be regarded as a burst with one spike [16]. Theoretical studies that performed fast-slow analysis of the effects of blocking the SK current in pancreatic β-cells [30, 34] and BK current in the case of pituitary somatotrophs and lactotrophs [10, 9, 12] clearly demonstrate that these effects are accompanied by changes in the location of the full-system equilibrium point. These studies also show that the position of the full-system equilibrium changes when voltage-gated Ca^{2+}-channel kinetics in a model of pituitary corticotrophs [7] or the conductance of A-type K^+-current in a model of pituitary lactotrophs [35] are varied. All of the above-mentioned theoretical studies not only demonstrated that such voltage dynamics perturbations affect the number of spikes and consequently the duration of the active phase, but also that these effects cannot be completely understood in terms of a classical fast-slow decomposition of the bursting model.

In this paper we addressed the question how the dynamics of plateau bursting depends on the location of the equilibrium point of the system. Since we focussed on fundamental, common features of plateau bursting we studied this dependence in a generic plateau-bursting model [16]. Typically, in endocrine cell models the location of the equilibrium depends on a number of parameters that define the properties of the ionic currents involved in bursting as well as the dynamics of the intracellular calcium concentration that regulates hormonal secretion. We showed how the bursting behaviour depends on the location of the full-system equilibrium point for both types of plateau bursting. Our analysis revealed that, indeed, the number of spikes within a burst depends on the position of this equilibrium, which may offer an explanation for the experimental observations mentioned above. Our results also clearly demonstrated the difference between depolarised continuous spiking and large-amplitude continuous spiking: the former is characterised by a planar sinusoidal nature and, thus, results in very small changes in the slow variable. In contrast, the latter has a relaxation oscillation character that is accompanied by significantly larger variations in the slow variable. This observation is important from a physiological point of view, because both dynamical regimes would presumably produce very different effects on secretion. Namely, small-amplitude continuous spiking would be more likely to provoke desensitisation and saturation effects, whereas large-amplitude spiking, that could be thought of as a burst with one spike, could allow for recovery processes to take place.

There are two main conclusions to draw from our results that contribute to the theory developed in [26, 24]. Firstly, the theory for the case with $s = -1.61$, where H is supercritical, is discussed in [26, 24] for a small neighbourhood in parameter space around the values for which FP is at HC and ε is small enough. Tonic spiking exists on one side of HC and bursting on the other side. A homoclinic bifurcation occurs at the transition from tonic spiking to bursting [24]. We studied this scenario by varying the parameter b_1, which moves the location of FP, and concentrated on the full range for b_1 where FP is unstable and lies well outside a neighbourhood of HC. This parameter range covers the regimes for tonic spiking and bursting that both originate in Hopf bifurcations at H_{FP} and $\mathsf{SH}_{\mathrm{FP}}$, respectively. The Hopf bifurcation

$\mathsf{SH}_{\mathrm{FP}}$ is singular and followed by a canard explosion that generates the bursting solutions. As we already reported in [16], the points H_{FP} and $\mathsf{SH}_{\mathrm{FP}}$ are connected via a curve of Hopf bifurcations in (ε, b_1)-space. We showed here that the two families of periodic orbits that emanate from H_{FP} and $\mathsf{SH}_{\mathrm{FP}}$ are also connected via b_1-dependent curves, but always via segments where the orbits are unstable as FP passes through HC; the connection may not happen via the primary tonic-spiking branch, but then it occurs at a period-doubled branch from a hierarchy of period-doubling bifurcations. As soon as such a connection exist, the branches at higher levels in the hierarchy also appear to connect, while the levels below this first connection consist of branches that end in homoclinic bifurcations. These homoclinic bifurcations are not all at the same point, but all lie in an $O(\varepsilon)$-neighbourhood of the b_1-value for which FP is at HC.

For $b_1 < 0$ close enough to 0, the bursting solutions are organised in n-spike families that are connected via pairs of SNPs, which increase the number of spikes. As b_1 decreases, the families of n-spike solutions form isolas that may overlap. The transition from connected families to isolas appears to be related to the position of FP relative to HC, which is consistent with earlier results presented in [16], where we used the speed ε of the slow variable as the primary bifurcation parameter.

Our second main result contributes to the case with $s = -2.6$, where H is subcritical. The organisation of the bursting patterns for this case has previously only been studied in [16]. Based on [16, 24], there exists no tonic spiking for b_1-values such that FP lies near HC, provided ε is small enough. Indeed, we found tonic spiking only for parameter regimes such that FP lies well outside a neighbourhood of HC. However, tonic spiking does exists, also for the subcritical case. In fact, the organisation of the transitions from tonic spiking to bursting are very similar to those for $s = -1.61$; the main differences are that the canard explosion at $\mathsf{SH}_{\mathrm{FP}}$ incorporates several spike-adding bifurcation such that the emering attracting bursting solution is a pseudo-plateau bursting orbit with several small-amplitude oscillations. Furthermore, the regime where tonic spiking is stable is much smaller. We remark that tonic spiking ends in a torus bifurcation for $s = -2.6$, but such torus bifurcations can also occur when s is such that H is supercritical. Indeed, the quasi-periodicity of the orbit has virtually no influence on the tonic spiking behaviour. Therefore, we conclude that, despite the vast difference between square-wave and pseudo-plateau bursting, the organisation of their bursting patterns is qualitatively the same.

Acknowledgements

HMO was supported by an Advanced Research Fellowship of the Engineering and Physical Sciences Research Council (EPSRC), UK.

References

[1] Vincent J, Kukstas L, Lledo P. Endocrine cell excitability opens the way to novel pharmacological intervention: example of the anterior pituitary cell. *Cell Biol Toxicol* 1992; **8**(3): 85–91.

[2] Van Goor F, Zivadinovic D, Martinez-Fuentes A, Stojilkovic SS. Dependence of pituitary hormone secretion on the pattern of spontaneous voltage-gated calcium influx. cell type-specific action potential secretion coupling. *J Biol Chem* 2001; **276**(36): 33840–33846.

[3] Barg S, Rorsman P. Insulin secretion: A high-affinity Ca^{2+} sensor after all? *J Gen Physiol* 2004; **124**(6): 623–625.

[4] Rinzel J. Bursting oscillations in an excitable membrane model. In *Lecture Notes in Mathematics*, Vol 1151. New York: Springer-Verlag, 1985: 304–316.

[5] Bertram R, Butte MJ, Kiemel T, Sherman A. Topological and phenomenological classification of bursting oscillations. *Bull Math Biol* 1995; **57**(3): 413–439.

[6] Izhikevich EM. Neural excitability, spiking and bursting. *Int J Bif Chaos* 2000; **10**(6): 1171–1266.

[7] LeBeau AP, Robson AB, McKinnon AE, Sneyd J. Analysis of a reduced model of cortiocotroph action potentials. *J Theoret Biol* 1998; **192**(3): 319–339.

[8] Van Goor F, Li Y, Stojilkovic SS. Paradoxical role of large-conductance calcium-activated K^+(BK) channels in controlling action potential-driven Ca^{2+} entry in anterior pituitary cells. *J Neurosci* 2001; **21**(16): 5902–5915.

[9] Tabak J, Toporikova N, Freeman M, Bertram R. Low dose of dopamine may stimulate prolactin secretion by increasing fast potassium currents. *J Comput Neurosci* 2007; **22**(2): 211–22.

[10] Tsaneva-Atanasova KT, Sherman A, Van Goor F, Stojilkovic SS. Mechanism of spontaneous and receptor-controlled electrical activity in pituitary somatotrophs: Experiments and theory. *J Neurophysiol* 2007; **98**(1): 131–144.

[11] Stern JV, Osinga HM, LeBeau AP, Sherman A. Resetting behavior in a model of bursting in secretory pituitary cells: distinguishing plateaus from pseudo-plateaus. *Bull Math Biol* 2008; **70**(1): 68–88

[12] Nowacki J, Mazlan SH, Osinga HM, Tsaneva-Atanasova KT. The role of large-conductance calcium-activated K^+ (BK) channels in shaping bursting oscillations of a somatotroph cell model. *Phys D* 2010; **239**(9): 485–493.

[13] Chay TR, Keizer J. Minimal model for membrane oscillations in the pancreatic beta-cell. *Biophys J* 1983; **42**(2): 181–189.

[14] Bertram R, Previte J, Sherman A, Kinard TA, Satin LS. The phantom burster model for pancreatic beta-cells. *Biophys J* 2000; **79**(6): 2880–2892.

[15] Tsaneva-Atanasova KT, Zimliki CL, Bertram R, Sherman A. Diffusion of calcium and metabolites in pancreatic islets: killing oscillations with a pitchfork. *Biophys J* 2006; **90**(10): 3434–3446.

[16] Tsaneva-Atanasova KT, Osinga HM, Rieß T, Sherman A. Full system bifurcation analysis of endocrine bursting models. *J Theoret Biol* 2010; online first DOI 10.1016/j.jtbi.2010.03.030.

[17] Booth V, Carr T, Erneux T. Near-threshold bursting is delayed by a slow passage near a limit point. *SIAM J Appl Math* 1997; **57**(5): 1406–1420.

[18] Shilnikov A, Kolomiets M. Methods of the qualitative theory for the Hindmarsh-Rose model: A case study. A tutorial. *Int J Bif Chaos* 2008; **18**(8): 2141–2168.

[19] Hindmarsh JL, Rose RM. A model of neuronal bursting using 3 coupled 1st order differential-equations. *Proc Roy Soc London Ser B — Biol Sci* 1984; **221**(1222): 87–102.

[20] Alexander JC, Cai DY. On the dynamics of bursting systems. *J Math Biol* 1991; **29**(5): 405–23.

[21] Terman D. Chaotic spikes arising from a model of bursting in excitable-membranes. *SIAM J Appl Math* 1991; **51**(5): 1418–1450.

[22] Mosekilde E, Lading B, Yanchuk S, Maistrenko Yu. Bifurcation structure of a model of bursting pancreatic cells. *Biosystems* 2001; **63**(1–3): 3–13.

[23] Bertram R, Sherman A. A calcium-based phantom bursting model for pancreatic islets. *Bull Math Biol* 2004; **66**(5): 1313–1344.

[24] Belykh VN, Belykh IV, Colding-Jørgensen M, Mosekilde E. Homoclinic bifurcations leading to the emergence of bursting oscillations in cell models. *The European Physical Journal E* 2000; **3**(3): 205–219.

[25] Desroches M, Guckenheimer J, Krauskopf B, Kuehn C, Osinga HM, Wechselberger M. Mixed-mode oscillations with multiple time scales. *submitted* 2010.

[26] Terman D. The transition from bursting to continuous spiking in excitable membrane models. *J Nonl Sci* 1992; **2**(2): 135–182.

[27] Doedel EJ. AUTO2000 and AUTO-07P: Continuation and bifurcation software for ordinary differential equations. Available from http://sourceforge.net/projects/auto2000, Concordia Univ., 2000. with major contributions from and Champneys AR, Fairgrieve TF, Kuznetsov YuA, Oldeman B, Sandstede B, Wang XJ.

[28] Beauvois MC, Merezak C, Jonas J-C, Ravier MA, Henquin J-C, Gilon P. Glucose-induced mixed $[Ca^{2+}]_c$ oscillations in mouse beta-cells are controlled by the membrane potential and the SERCA3 Ca^{2+}-ATPase of the endoplasmic reticulum. *Am J Physiol Cell Physiol* 2006; **290**(6): C1503–1511.

[29] Guckenheimer J, Kuehn C. Computing slow manifolds of saddle type. *SIAM J Appl Dyn Sys* 2009; **8**(3): 854–879.

[30] Chay TR, Rinzel J. Bursting, beating, and chaos in an excitable membrane model. *Biophys J* 1985; **47**: 357–366.

[31] Wang X-J. Genesis of bursting oscillations in the Hindmarsh-Rose model and homoclinicity to a chaotic saddle. *Phys D* 1993; **62**(1–4): 263–274.

[32] Vergara L, Rojas L, Stojilkovic SS. A novel calcium-activated apamin-insensitive potassium current in pituitary gonadotrophs. *Endocrinology* 1997; **138**(7): 2658–2664.

[33] Zhang M, Houamed K, Kupershmidt S, Roden D, Satin LS. Pharmacological properties and functional role of K_{slow} current in mouse pancreatic β-Cells: SK channels contribute to K_{slow} tail current and modulate insulin secretion. *J Gen Physiol* 2005; **126**(4): 353–363.

[34] Chay TR. On the effect of the intracellular calcium-sensitive K^+channel in the bursting pancreatic β-cell. *Biophys J* 1986; **50**(5): 765–777.

[35] Toporikova N, Tabak J, Freeman M, Bertram R. A-type K^+current can act as a trigger for bursting in the absence of a slow variable. *Neural Comput* 2008; **20**(2): 436–451.

[36] Polderman JW, Willems JC. *Introduction to Mathematical Systems Theory. A Behavioral Approach*. Vol 26 of Texts in Applied Mathematics. New York: Springer-Verlag, 1998.

Appendix

The analysis of the fast subsystem of (1) can largely be done explicitly. Recall that the fast subsystem of (1) is given by

$$\left\{ \begin{array}{rcll} \dot{x} & = & f(x,y,z) & := \quad s\,a\,x^3 - s\,x^2 - y - b\,z, \\ \dot{y} & = & g(x,y) & := \quad x^2 - y, \end{array} \right. \tag{2}$$

where z is considered a parameter. Note that we ignore the time-scale separation in x and y and assume $\phi = 1$ in (1). The z-family of equilibria of (2) are given as a function of $x \in \mathbb{R}$. Indeed, by setting the right-hand sides of (2) to zero, we find that for each $x \in \mathbb{R}$ an equilibrium exists with this x-coordinate and y-coordinate

$$y = x^2, \tag{3}$$

at the parameter value

$$z = \frac{s\,a\,x^3 - s\,x^2 - y}{b} = \frac{s\,a\,x^3 - (s+1)\,x^2}{b}. \tag{4}$$

Due to the cubic nature of the equation for z, we indeed get the required Z-shaped curve of equilibria as a function of z, provided $s\,a \neq 0$ and $s \neq -1$. The local maxima and minima of z are the fold points along the Z-shaped curve of equilibria, but we derive these in the standard way as follows.

For each $x \in \mathbb{R}$, the Jacobian at the corresponding equilibrium point is given by

$$\mathrm{Jac}(x) := \begin{bmatrix} 3\,s\,a\,x^2 - 2\,s\,x & -1 \\ 2\,x & -1 \end{bmatrix}.$$

Fold points are characterised by a zero eigenvalue of $\mathrm{Jac}(x)$. We find

$$\begin{aligned} \det(\mathrm{Jac}(x)) = 0 &\Leftrightarrow -3\,s\,a\,x^2 + 2\,s\,x + 2\,x = 0 \\ &\Leftrightarrow 2\,(s+1)\,x - 3\,s\,a\,x^2 = 0 \\ &\Leftrightarrow x = 0 \quad \text{or} \quad x = \frac{2\,(1+s)}{3\,s\,a}. \end{aligned} \tag{5}$$

Using the equilibrium conditions (3) and (4) for the corresponding y- and z-coordinates, we find that the fold points in (x, y, z)-space are given by

$$\begin{aligned} \mathsf{SN}_1 &:= (0, \quad 0, \quad 0), \\ \mathsf{SN}_2 &:= \left(\frac{2\,(1+s)}{3\,s\,a}, \quad \frac{4\,(1+s)^2}{9\,s^2\,a^2}, \quad \frac{-4\,(1+s)^3}{27\,s^2\,a^2\,b}\right). \end{aligned}$$

The equilibrium FP of the full system (1) lies exactly at a fold point if b_1 is such that the right-hand side of the z-equation of system (1) gives zero for such a triple of (x, y, z)-values. That is, b_1 is found as

$$\varepsilon(s\,a_1\,x + b_1 - k\,z) = 0 \Leftrightarrow s\,a_1\,x + b_1 - k\,z = 0 \Leftrightarrow b_1 = k\,z - s\,a_1\,x. \tag{6}$$

The Hopf bifurcation point is found in a similar way. A Hopf bifurcation is characterised by a pair of purely imaginary eigenvalues. Hence, we must have $\det(\mathrm{Jac}(x)) > 0$ and

$$\begin{aligned} \mathrm{trace}(\mathrm{Jac}(x)) = 0 &\Leftrightarrow 3\,s\,a\,x^2 - 2\,s\,x - 1 = 0 \\ &\Leftrightarrow x = \frac{s \pm \sqrt{s^2 + 3\,s\,a}}{3\,s\,a}. \end{aligned} \tag{7}$$

Using the fact that $\mathrm{trace}(\mathrm{Jac}(x)) = 0$, the inequality $\det(\mathrm{Jac}(x)) > 0$ simply reduces to $x > \frac{1}{2}$. For our choice of the parameters $a = 0.5 > 0$ and $s = -1.61$ or $s = -2.6$, that is, $s < 0$, we require

$$\begin{aligned} \det(\mathrm{Jac}(x)) > 0 &\Leftrightarrow s \pm \sqrt{s^2 + 3\,s\,a} < \frac{3\,s\,a}{2} \\ &\Leftrightarrow \pm\sqrt{s^2 + 3\,s\,a} < \frac{(3\,a - 2)\,s}{2}. \end{aligned}$$

Since $3\,a - 2 = -0.5 < 0$ for $a = 0.5$, the right-hand side of this inequality is positive and the solution with the $-$ sign in (7) is always a Hopf bifurcation, as long as the square-root term is real, that is, $s < -3\,a$. A second Hopf bifurcation exists only if

$$s \geq \frac{4\,a}{3\,a^2 - 2\,a - 1},$$

which is $s = -1.6$ in our setting and corresponds to a Bogdanov-Takens point; since we want to have only one Hopf bifurcation on the upper branch of the Z-shaped curve of equilibria of

system (1), we need $s < -1.6$. In this case, using (3) and (4), the unique Hopf bifurcation is given by

$$\mathsf{H} := \left(\frac{s - \sqrt{\mathsf{D}}}{3\,s\,a}, \quad \frac{2\,s + 3\,a - 2\,\sqrt{\mathsf{D}}}{9\,s\,a^2}, \quad \frac{-2\,s^2 - 6\,s - 9\,a + (2\,s - 3\,a + 6)\,\sqrt{\mathsf{D}}}{27\,s\,a^2\,b} \right),$$

where $\mathsf{D} = \sqrt{s^2 + 3\,s\,a}$. We find the corresponding b_1-value by using the x- and z-coordinates of H for x and z in (6).

The stability of FP is determined by the eigenvalues of the Jacobian of the full system (1). The characteristic polynomial of FP is of the form

$$\mathrm{char}_{\mathrm{FP}}(\xi) = \xi^3 + c_2\,\xi^2 + c_1\,\xi + c_0,$$

with

$$\begin{aligned} c_2 &= \varepsilon\,k + 1 - 3\,s\,a\,x_{\mathrm{FP}}^2 + 2\,s\,x_{\mathrm{FP}}, \\ c_1 &= (\varepsilon\,k + 1)\,(1 - 3\,s\,a\,x_{\mathrm{FP}}^2 + 2\,s\,x_{\mathrm{FP}}) - 1 + 2\,x_{\mathrm{FP}} + \varepsilon\,s\,a_1 b, \\ c_0 &= \varepsilon\,k\,(2\,x - 3\,s\,a\,x_{\mathrm{FP}}^2 + 2\,s\,x_{\mathrm{FP}}) + \varepsilon\,s\,a_1 b. \end{aligned}$$

Here, x_{FP} is the x-coordinate of FP, which is determined by the choice for b_1. The Routh-Hurwitz criterion [36] states that FP is stable if and only if the coefficients are all positive and $c_1\,c_2 - c_0 > 0$. In particular, the characteristic polynomial of FP for $b_1 = 0$, that is, when FP lies on SN_1, is given by

$$\mathrm{char}_{\mathsf{SN}_1}(\xi) = \xi^3 + (1 + \varepsilon\,k)\,\xi^2 + \varepsilon\,(k + a_1 b\,s)\,\xi + \varepsilon\,a_1 b\,s.$$

Notice that all coefficients are positive for our choices of $k = 0.2$, $a_1 = -0.1$ and $b = 1$, since we assume $s < -1.6$. Moreover,

$$c_1\,c_2 - c_0 = \varepsilon\,(k + a_1 b\,s)\,(1 + \varepsilon\,k) - \varepsilon\,a_1 b\,s = \varepsilon\,k\,(1 + \varepsilon\,k + \varepsilon\,a_1 b\,s) > 0.$$

Hence, FP is always stable for $b_1 \geq 0$, irrespective of the choices for $s < -1.6$ and $\varepsilon > 0$, and $\mathsf{SH}_{\mathrm{FP}}$ can only occur for $b_1 < 0$.